Fragile three-dimensionality in the quasi-one-dimensional cuprate $PrBa_2Cu_4O_8$

A Narduzzo[1], A Enayati-Rad[1], P J Heard[2], S L Kearns[3], S Horii[4], F F Balakirev[5] and N E Hussey[1]

[1] H. H. Wills Physics Laboratory, University of Bristol, Tyndall Avenue, Bristol, BS8 1TL, UK

[2] Interface Analysis Centre, Oldbury House, 121 St. Michael's Hill, Bristol, BS2 8BS, UK

[3] Department of Earth Sciences, University of Bristol, Wills Memorial Building, Queen's Road, Bristol, BS8 1RJ, UK

[4] Department of Applied Chemistry, University of Tokyo, 7-3-1 Hongo, Bunkyo-ku, Tokyo, 113-8656, Japan

[5] National High Magnetic Field Laboratory, Los Alamos National Laboratory, Los Alamos, New Mexico, 87545, USA

E-mail: n.e.hussey@bristol.ac.uk

Abstract. In this article we report on the experimental realization of dimensional crossover phenomena in the chain compound $PrBa_2Cu_4O_8$ using temperature, high magnetic fields and disorder as independent tuning parameters. In purer crystals of $PrBa_2Cu_4O_8$, a highly anisotropic three-dimensional Fermi-liquid state develops at low temperatures. This metallic state is extremely susceptible to disorder however and localization rapidly sets in. We show, through quantitative comparison of the relevant energy scales, that this metal/insulator crossover occurs precisely when the scattering rate within the chain exceeds the interchain hopping rate(s), i.e. once carriers become confined to a single conducting element.

PACS numbers: 71.27.+a, 71.30.+h, 72.15.Rn

1. Introduction

There is growing evidence that in compounds containing isolated atomic [1] or molecular [2] chains, the conventional Fermi-liquid picture of electron-like quasiparticles fails. How the corresponding one-dimensional state [3, 4] of decoupled spin and charge excitations emerges however remains unresolved, prompting the search for compounds whose electronic ground state can be tuned progressively towards one-dimensionality. In metals on the boundary of one-dimensionality, the so-called quasi-one-dimensional (quasi-1D) conductors, the Fermi surface takes the form of pair(s) of parallel corrugated sheets in the plane normal to the conducting chain(s). Provided the two orthogonal interchain hopping energies $2t_\perp$ (which determine the size of corrugation in each direction) are larger than other relevant perturbations, hopping between chains is coherent and in the absence of charge ordering, a 3D Fermi-liquid ground state is stabilized at low temperature. If this corrugation is 'smeared out' and the chains become decoupled however, theory predicts [3, 4] that even weak interactions will drive the system into the 1D Luttinger-liquid state with its associated phenomenon of spin-charge separation. In order to realize and study the crossover between these two extreme ground states, it is necessary to identify materials where $2t_\perp$ in both directions is restricted, due to orbital overlap or correlation effects, to energies attainable within the laboratory.

$PrBa_2Cu_4O_8$ (Pr124) is the non-superconducting analogue of the high-temperature superconductor $YBa_2Cu_4O_8$ (Y124). Its crystal structure, shown in Fig. 1), consists of edge-sharing double CuO chain networks (oriented along the crystallographic *b*-axis) sandwiched between sets of CuO_2 bilayer plaquettes. Substitution of Pr for Y between the bilayers completely suppresses superconductivity (and mobility) within the CuO_2 planes [5] whilst preserving the metallicity of the double chains [6, 7]. This offers a unique opportunity to study the charge dynamics of the cuprate chain in isolation. In this article, we show that temperature, magnetic fields and disorder can all induce a 3D to 1D crossover in the electronic ground state of Pr124 under laboratory conditions. Whilst dimensional crossover phenomena due to high temperatures [8, 9], high magnetic fields [10, 11, 12] and even strong correlation effects [13] have been well documented, to our knowledge, this is the first experimental realization of *disorder*-induced one-dimensionality in a three-dimensional compound.

2. Methods

2.1. Crystal growth and characterisation

Single crystals of $PrBa_2Cu_4O_8$ were grown by a self-flux method in MgO crucibles under high-pressure oxygen gas of 11atm [7]. The impurity content of three of the crystals used in the disorder study was investigated by means of secondary-ion mass spectrometry (SIMS) as well as electron probe micro-analysis (EPMA). SIMS identified a number of trace impurity elements (including Fe but not Ni or Co) but only three, Mg, Al and Sr, had abundances above the detectability limit of our EPMA measurements (100ppm).

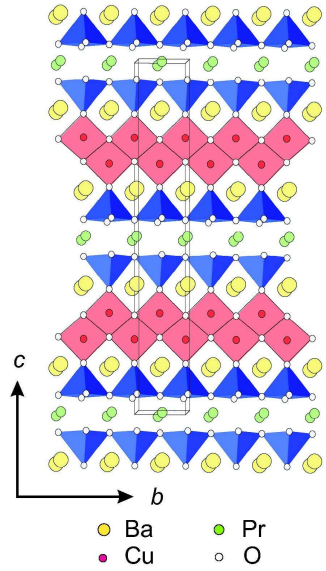

Figure 1. Schematic of the crystallographic structure of Pr124. The red squares represent the CuO double chain network oriented along the b-axis. The unit cell is indicated by a thin solid line.

Of these, Mg was by far the most abundant, as expected through contamination with the crucible walls.

2.2. Zero- and pulsed-field resistivity measurements

The resistivities were measured using a standard four-probe ac lock-in technique. For the $\rho_c(T, B)$ measurements, electrical contacts were mounted on the top surfaces of the crystal whilst for the $\rho_a(T, B)$ measurements, they were mounted on the corners. In each case, the other highly resistive direction was shorted out to ensure uniaxial current flow. For in-chain resistivity (ρ_b) measurements, the crystal dimensions were recorded using a scanning electron microscope. In addition, voltage contacts were placed so as to avoid contamination from the two other highly resistive current directions. An example of the voltage contact configuration for ρ_b measurements is shown in Fig. A.1) of the Appendix. Due to the smallness of the samples and the finite width of the voltage electrodes, the convention adopted in estimating their distance plays an important role in the determination of the absolute resistivity values. In this study, we have taken the midpoint of the wire (diameter 25 μm) at the sample as the marker for the electrode position. Uncertainties in our estimates of the sample dimensions are 10-15%. In previous studies [12, 14, 15], different markers have been used. As discussed in the Appendix, we believe this choice of marker is primarily responsible for the large discrepancies in the absolute magnitudes of the ρ_b values reported in the literature.

The high field measurements were performed in the 65 Tesla pulsed magnet at the NHMFL, Los Alamos, USA. A typical 100 ms long magnetic field pulse is produced by discharging 1.6 MJ capacitor bank through a reinforced copper alloy magnet coil.

Resistance versus magnetic field is recorded again using a standard high frequency lock-in technique.

3. Temperature and Magnetic Field Induced Dimensional Crossover Phenomena in Pr124

It was shown previously [14] that in high-quality Pr124 crystals, electrical resistivity at low T is metallic in all three orthogonal directions and varies approximately as T^2, consistent with the development of a 3D Fermi-liquid ground state. The resistive anisotropy at low T however is extremely large ($\rho_a : \rho_b : \rho_c(T = 0) \sim 1000 : 1 : 3000$) [14], with a similar anisotropy in the ratio of the (squares of the) hopping energies. Moreover, whilst $\rho_b(T)$ in the purest crystals remains metallic for all $T < 300$K, the interchain resistivities $\rho_a(T)$ and $\rho_c(T)$ have maxima around $T = 150$K above which their behaviour becomes thermally activated. These maxima have been interpreted either as a 3D to 1D crossover with increasing temperature or as the emergence of a contribution to $\rho_{a,c}(T)$ from the insulating CuO_2 planes.

Dimensional crossover phenomena can also be realized in high magnetic fields, due to a field-induced real-space confinement of the charge carriers [17]. In the double-chain cuprate Pr124, the Fermi surface consists of two pairs of corrugated sheets extending normal to the reciprocal space axis $\mathbf{k}_b$. Within a simple tight-binding picture, the c-axis dispersion (for a single chain) is $\mathcal{E} = -2t_\perp^c cos(k_c c)$. For $B \parallel a$, the dominant Lorentz force $e[\mathbf{v}_F \times \mathbf{B}] = ev_F B\hat{\mathbf{c}} = \hbar d\mathbf{k}_c/dt$ causes carriers to traverse the Fermi sheet along k_c. The sinusoidal corrugation then gives rise to an oscillatory component to the c-axis velocity $v_\perp^c = \hbar^{-1}[\partial\mathcal{E}_\perp^c/\partial k_z] = [2t_\perp^c c/\hbar]sin(k_c c)$ and hence to a real-space sinusoidal trajectory with amplitude $A_c = 2t_\perp^c/ev_F B$. Thus A_c shrinks as B increases until eventually at $B_{\rm cr}^c = 2t_\perp^c/ev_F c$, $A_c = c$ and the charge carriers become confined to a single plane of coupled chains. Note that $B_{\rm cr}^c$ is independent of $1/\tau$ and therefore independent of temperature and impurity concentration, as verified experimentally [12, 16]. Due to the quasi-1D nature of the Fermi sheets in Pr124, a similar oscillatory component of amplitude $A_a = 2t_\perp^a/ev_F B$ will also be induced along the a-axis for $B \parallel c$. In this case, the crossover field is expected to occur at $B_{\rm cr}^a = 2t_\perp^a/ev_F a$.

Figure 2a) shows transverse field sweeps of the c-axis resistivity $\rho_c(B)$ (transverse to both the current and the conducting chain) at different fixed temperatures. The inset shows a blow-up of the low-field region (enclosed by a solid rectangle in Fig. 2a), minus the 40K data for clarity). Below a crossing field $B_{\rm cr}^c$ (= 10(1) Tesla, shown by a dashed line), $\rho_c(T)$ is metallic. Above $B_{\rm cr}^c$ however, the trend is reversed, implying a metallic/non-metallic crossover in the interchain resistivity as a function of field. (For more details on the precise determination of $B_{\rm cr}^c$, please refer to Ref. [12]). As shown in Fig. 2b), a similar phenomenon occurs in the reciprocal configuration ($B \parallel c$, $I \parallel a$), though here the corresponding crossover field is extremely high, $B_{\rm cr}^a = 62(2)$ Tesla. This is due principally to the fact the $a \sim c/3$ and therefore a much larger field is required to confine the electrons along the a-axis.

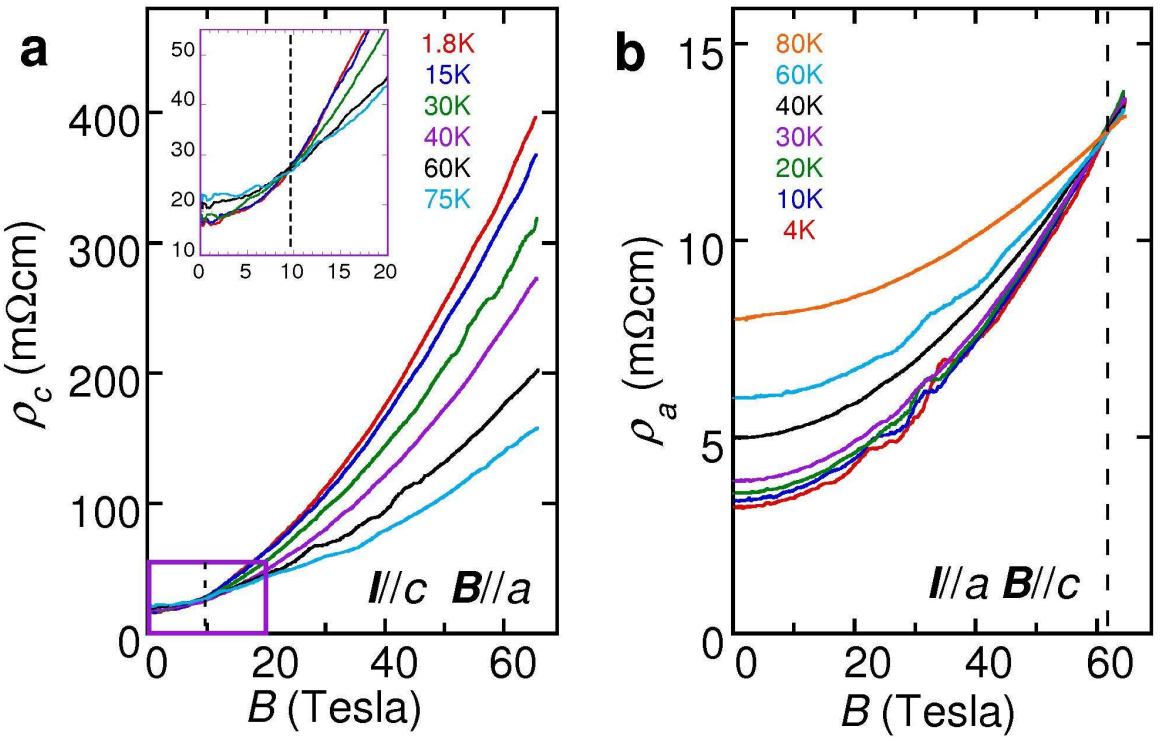

Figure 2. **a)** Transverse field sweeps of the c-axis resistivity $\rho_c(B)$ (transverse to both the current and the conducting chain) at different fixed temperatures. The inset shows a blow-up of the low-field region (enclosed by a solid rectangle in Fig. 1a), minus the 40K data for clarity). The dashed line indicates the crossover field $B^c_{\rm cr}$ (see main text). **b)** Transverse field sweeps of the a-axis resistivity $\rho_a(B)$. Again the dashed line indicates the crossover field $B^a_{\rm cr}$.

From the crossover fields in the transverse B sweeps shown in Fig. 2a) - b), we obtain $2t^c_\perp \sim 45(5)$K and $2t^a_\perp \sim 70(2)$K. We can now compare these values with estimates of $2t_\perp$ from the T-dependent resistivity data. Fig. 3a) and 3b) show $\rho_c(T)$ and $\rho_a(T)$ data respectively for the same crystals that were used in the magnetic field study. Typically, there are two energy scales that are used as a measure of $2t_\perp$ in the interplane(chain) resistivities of low-dimensional metals; the peak in $\rho_\perp(T)$ at $T^{a,c}_{\rm max}$ is generally regarded as an upper bound for $2t_\perp$ whilst the deviation from the low-T quadratic resistivity gives a lower bound. In Sr_2RuO_4 for example, the latter criterion has been shown to give very consistent agreement with the value of $2t_\perp$ estimated for the most conducting band from quantum oscillation experiments [18]. The insets in Fig. 3a) and 3b) show $\rho_{c,a}(T)$ versus T^2 below $T = 70$K and $T = 110$K respectively. The arrows indicate the temperatures $T^{a,c}_{\rm coh}$ at which $\rho_{a,c}(T)$ first deviates from T^2. From these plots we find $T^a_{\rm coh} = 70(5)$K, $T^a_{\rm max} = 130$K, $T^c_{\rm coh} = 50(5)$K and $T^c_{\rm max} = 180$K. Note that the $T^{a,c}_{\rm coh}$ values are in excellent agreement with the values for $2t_\perp$ determined from the two sets of magnetic field measurements. From this we conclude that $T^{a,c}_{\rm coh}$ defines the temperature at which a,c-axis hopping first begins to lose coherence (i.e. when $k_{\rm B}T \sim 2t_\perp$). The peaks, in contrast, appear to represent the temperature at which all

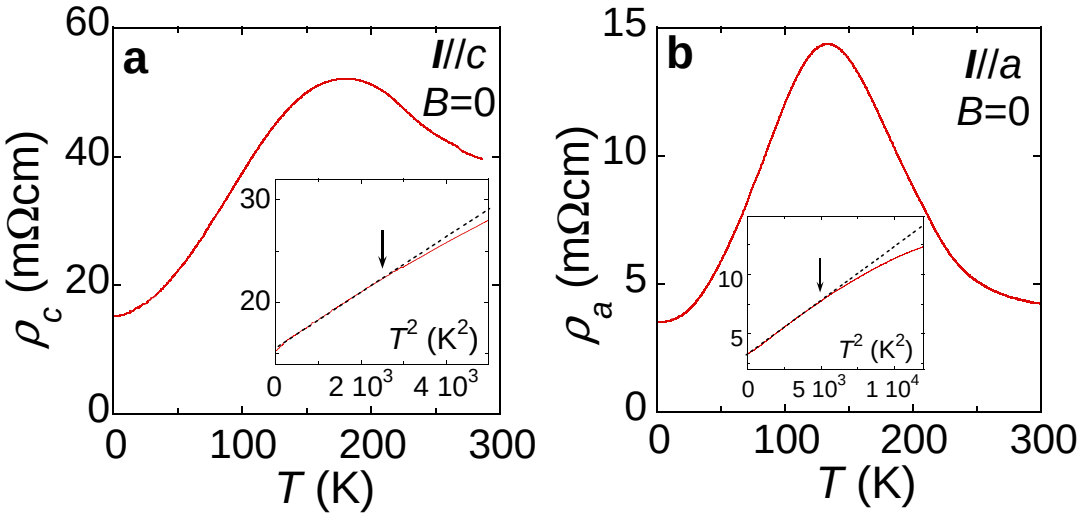

Figure 3. a) $\rho_c(T)$ for the same crystal as in Fig. 2a); the inset shows $\rho_c(T)$ versus T^2 below $T = 70$K. The arrow indicates the temperature $T^c_{\rm coh} = 50(5)$K at which $\rho_c(T)$ first deviates from T^2. The kink in $\rho_c(T)$ at low T is due to the Pr ordering at $T = T_{\rm N}$. **b)** $\rho_a(T)$ for the same crystal as in Fig. 2b); in the inset, $\rho_a(T)$ plotted versus T^2 below $T = 110$K. Here $T^a_{\rm coh} = 70(5)$K (again indicated by an arrow).

interchain coherence is lost. In the temperature range $T^{a,c}_{\rm coh} \leq T \leq T^{a,c}_{\rm max}$ therefore, the chains are very weakly coupled and metallicity is seen to disappear only gradually.

4. Disorder-induced localization in Pr124

We now turn our attention to the intrachain current response. Fig. 4a) shows $\rho_b(T)$ data for four needle-shaped samples $b1-4$ taken from the same growth batch. At high T, $\rho_b(T)$ is metallic and quasi-linear, the slopes being similar in all four samples suggesting uniform carrier concentration. Only $b1$ however remains metallic down to the lowest temperature studied ($T = 0.5$K). For $b1$, $\rho_b(T) = \rho_{0b} + AT^\alpha$ below 100K. The coefficient $\alpha = 2.3$ falls within the expected range ($2 < \alpha < 3$) for a quasi-1D Fermi-liquid with dominant electron-electron scattering [27]. The other samples have minima at $T = T_{\rm min}$ below which $\rho_b(T)$ gradually increases. Fig. 4b) shows a blow-up of the low-T resistivity data for $b2$, located right at the boundary between the metallic and non-metallic behaviour. The kink in $\rho_b(T)$ at $T_N = 17$K indicated by an arrow coincides with the antiferromagnetic ordering of the Pr ions [19]. In $b3$ and $b4$, this kink manifests itself as a change of slope. Intriguingly, in *all* crystals that exhibit metallic behaviour down to low T (i.e. those with low residual resistivities, including $b1$), $\rho_b(T)$ appears unaffected by the Pr ordering.

Several mechanisms for the low T insulating behaviour, including variable range hopping [20], Kondo spin scattering [21], the charge Kondo effect [22], the $\ln(1/T)$ dependence observed in underdoped 2D cuprates [23] and the exponential behaviour expected for a Mott insulator [24], were considered but found to be incompatible with

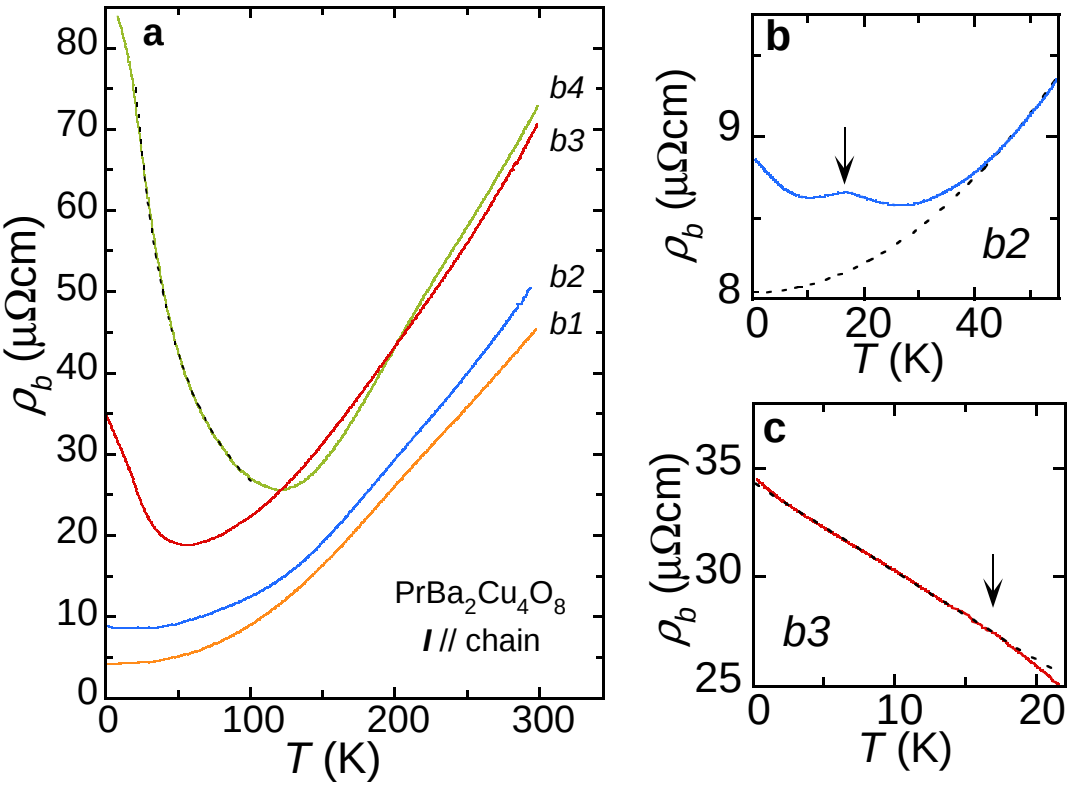

Figure 4. **a)** Zero-field $\rho_b(T)$ data for four single crystals with different levels of disorder. The dashed line overlaying the data of sample $b4$ is a fit to $\rho_b(T) = AT^{-2/3}$. **b)** Blow-up of the low-T $\rho_b(T)$ data for sample $b2$, on the boundary between metallicity and localization. The dashed line is an extrapolation of the metallic T^2 dependence between 45K and 60K. The arrow indicates the antiferromagnetic ordering temperature T_N of the Pr ions. **c)** Blow-up of the low-T $\rho_b(T)$ data for sample $b3$, highlighting the anomalous $-T$ behaviour below T_N (again marked by an arrow).

$\rho_b(T)$, both above and below T_N. Whilst Fe concentrations below 100ppm can give rise to resistivity upturns [25], we note here that the in-chain magnetoresistance behaviour of all four of these crystals is inconsistent with Kondo scattering [26]. Moreover Mg was the only element whose concentrations were found to scale with the size of the resistivity upturns; Mg_{b2} :Mg_{b3} :Mg_{b4} = 3500 : 4200 : 4700 (ppm). We therefore conclude that magnetic impurities were not responsible for the upturns in $\rho_b(T)$.

The large increase in $\rho_b(T)$ of $b3$ and $b4$ below $T_{\rm min}$ argues against weak localization, whilst the very gradual nature of the upturn in $\rho_b(T)$ suggests a lack of charge ordering in Pr124, most probably due to the stabilizing presence of the CuO_2 planes. The form of $\rho_b(T)$ for $T_{\rm N} < T < T_{\rm min}$ is best represented by a power law, (e.g. dashed line in Fig. 4a) for $b4$ where $\rho_b(T)$ varies as $T^{-2/3}$). Below $T_{\rm N}$ however, the T-dependence of $\rho_b(T)$ changes abruptly in all insulating samples. As illustrated in Fig. 4c) for sample $b3$ for example, $\rho_b(T)$ increases approximately linearly with decreasing T over a decade in temperature between 0.8K and 17K. The Néel ordering of the Pr ions thus splits the insulating behaviour into two disparate forms, one above $T_{\rm N}$ which is divergent, and

one below which is not, thereby making it difficult to identify the intrinsic transport behaviour in the insulating state.

For a quasi-1D metal, the residual resistivity ρ_{0b} is independent of carrier density. Hence ρ_{0b} can be used to obtain a direct measure of the intrachain mean-free-path ℓ. Given that $b2$ lies on the threshold between metallicity and localization, we can therefore extract an upper bound for the nominal mean-free-path $\ell_{\rm cr}$ at the metal/insulator boundary by extrapolating $\rho_b(T)$ of $b2$ from high T down to $T = 0$K. The dashed line in Fig. 4b) is an extrapolation of the metallic T^2 dependence between 45K and 60K. From this we obtain, $\rho_{0b} \leq 8(1)\mu$cm, giving $\ell_{\rm cr} \geq 215(25)\mathring{A}$. (Note that there are 2 chains per unit cell in Pr124, and so $\rho_{0b} = \pi ac\hbar/4e^2\ell$, where a ($= 3.88\mathring{A}$) and c ($= 13.6\mathring{A}$) are the a- and c-axis lattice constants respectively.) Since the b-axis lattice constant $b = 3.90\mathring{A}$, this is equivalent to more than 50 unit cells. Finally, taking estimates of the Fermi wave vector k_F ($= 0.2\ \mathring{A}^{-1}$) from angle-resolved photoemission spectroscopy (ARPES) [28], we arrive at $k_F\ell_{\rm cr} \geq 45(5)$ at the localization threshold. It is important to stress that independent estimates of $\ell_{\rm cr}$ from transverse interchain magnetoresistance measurements *that are insensitive to any uncertainties in the crystal dimensions and contact configurations* agree very well with the value extracted from ρ_{0b} of sample $b2$, thus supporting the convention for voltage markers adopted here.

Localization at such large values of $k_F\ell$ is unprecedented. In 3D Fermi-liquids for example, coherent (Bloch) electron motion is destroyed once $k_F\ell < 1$, corresponding to a mean-free-path shorter than the de Broglie wavelength. In the normal state of the 2D cuprates, the localization threshold occurs for $k_F\ell < 10$ [23], though its origin is as yet unknown. To our knowledge there have been no corresponding experimental studies of the localization threshold in quasi-1D systems. Extensive theoretical studies however have predicted that an insulating phase develops in a *strictly* 1D system for a vanishingly small amount of random impurities [29, 30, 31, 32]. The tendency towards localization in sample $b2$ at $k_F\ell_{\rm cr} \geq 45(5)$ suggests therefore that a fundamental change in the dimensionality of the electronic system has occurred and indeed, direct comparison of the relevant energy scales confirms this to be the case.

5. Discussion

According to ARPES [28], the Fermi velocity within the chains $v_F = 2.5 \times 10^5$ ms^{-1}. Thus the intrachain scattering rate at the localization threshold $\hbar/\tau_{\rm cr} = \hbar v_F/\ell_{\rm cr} \leq 80(10)$K. As discussed above, $2t_\perp^{a,c}$ (as determined from $B_{\rm cr}^{a,c}$) is also proportional to v_F. Thus direct comparison of the three energy scales ($2t_\perp^a$, $2t_\perp^c$ and $\hbar/\tau_{\rm cr}$) is in fact independent of the value of v_F. It is clear therefore that at the localization threshold, $\hbar/\tau$ is comparable to both orthogonal hopping energies. In this circumstance, intrachain scattering becomes sufficient to block coherent wave propagation between chains, making them decoupled electronically; the presence of arbitrary disorder within the (effectively isolated) chains then leads immediately to localization at the lowest temperature, as predicted [29, 30, 31, 32].

As mentioned in the previous section, the form of $\rho_b(T)$ for $T_N < T < T_{min}$ is best represented by a power law, (e.g. dashed line in Fig. 4a) for $b4$ where ρ_b varies as $T^{-2/3}$). Whilst this is consistent with predictions for a Luttinger liquid [24], it should be stressed that the T-range is too limited to make any concrete claims. Nevertheless, recent optical [33] and ARPES [34] results do support the emergence of Luttinger-liquid behaviour in Pr124, either in pure Pr124 at high T (i.e. when $k_BT > 2t_\perp^{a,c}$) or in Zn-doped Pr124 at low T (presumably when $\hbar/\tau > 2t_\perp^{a,c}$, though there no quantitative estimates of the energy scales were made). From both these studies, the Luttinger parameter K_ρ is estimated to be ~ 0.24, a value compatible [24] with the observation of a quasi-linear T-depenendence in $\rho_b(T)$ at high T, if one assumes a carrier concentration close to, but not quite, 1/4-filling. Significantly the resistivity data do not exhibit the exponential behaviour expected for a 1D Mott insulator at low T [24]. The small value of K_ρ suggests that this is due to deviations from commensurability, rather than to the absence of strong interactions.

6. Conclusions

In this article, we have reported supporting evidence for the first experimental realization of disorder-induced one-dimensionality in a 3D solid at low temperatures. This has only been made possible in Pr124 due to the extremely small values of $2t_\perp$ ($\leq$ 70K) in *both* perpendicular directions. In the quasi-1D organic conductors, such 3D to 1D crossover phenomena are extremely difficult to induce (at low T) due to the large coupling in the second direction (in $(TMTSF)_2PF_6$ for example, $2t_\perp^b \sim$ 600K [13]). This makes Pr124 a rather unique bulk system with which to study physical phenomena on the boundary between Fermi-liquid and Luttinger-liquid ground states that complements existing work on chiral edge states in 2D heterostructures [35]. Whilst it appears that disorder allows the manifestation of one-dimensionality in Pr124 at low T, it is, by its very nature, one displaying localized behaviour. Nevertheless, our results highlight one possible route to a delocalised Luttinger-liquid at low T, in ultra-pure Pr124 under a tilted (pulsed) magnetic field with components in the ac plane larger than the two crossover fields $B_{cr}^{a,c}$. Should such field-induced confinement also lead to an insulating state, then the paradigm that all states are localized in real 1D systems will gain yet more empirical confirmation. Finally, let us remark on the observation that the dimensional crossovers in Pr124 appear to occur once the strength of a particular perturbation, e.g. temperature T, magnetic field B, or scattering rate $1/\tau$, exceeds $2t_\perp$. This contrasts markedly with recent studies on quasi-2D conductors where evidence for interlayer coherence is observed despite the fact that both k_BT and $\hbar/\tau \gg 2t_\perp$ [36]. Clearly the phenomenon of interlayer or interchain decoherence in anisotropic metals is still poorly understood and it is only through further systematic studies that this important issue can be resolved.

Acknowledgments

We acknowledge S. Andergassen, C. Capan, A. Carrington, R. Claessen, T. Enss, T. Giamarchi, S. M. Hayden, S. Kivelson, N. Shannon, I. Terasaki, V. Tripathi and J. A. Wilson for their helpful comments. We also thank K. Nozawa and J. Hart for technical assistance. This work was supported by the EPSRC (UK). SH was financially supported by the Leverhulme Fellowship (UK). The work at the NHMFL was supported by the National Science Foundation and DOE Office of Science.

Appendix A.

We address here the issue of the determination of absolute values of the chain resistivity ρ_b. This requires an accurate measurement of crystal dimensions and of distances between contacts. With a high power optical microscope crystal dimensions can be known to a reasonable degree of accuracy, 20-25%, and with an SEM, significantly better than that. The chief source of systematic error is the large size of the electrical (voltage) contacts relative to their separation. In order to ensure uniaxial current flow in these highly anisotropic crystals it is necessary to coat conductive paint across the entire sample in both directions perpendicular to the current flow. This invariably leads to large contact pads relative to the sample dimensions. Moreover, it is not obvious which criterion one should use for specifying the distance between the voltage contacts in calculating the resistivity values. It depends to a large extent on the contact resistance of each pad and where within the pad the best electrical contact is made. A convention needs to be adopted by associating a marker with each contact pad. As an example of the importance of the marker scheme, Fig. A1 shows two SEM pictures of the voltage contacts for samples $b2$ and $b3$.

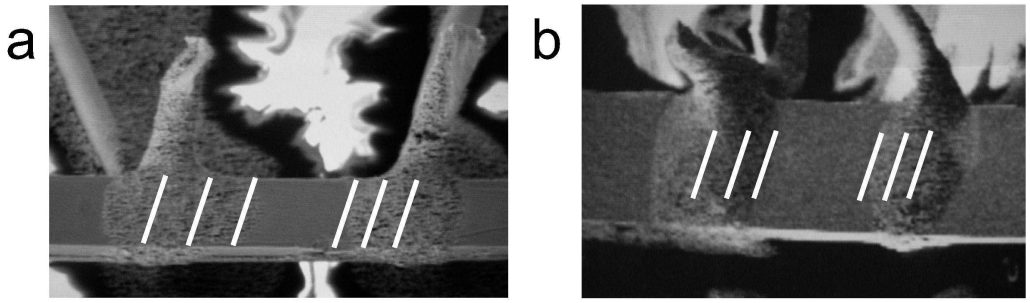

Figure A1. a) SEM picture of the pair of voltage contacts for sample $b2$. The white lines represent different markers used to determine the distance between contacts. **b)** A similar picture for sample $b3$. Using the markers at the mid-point of the Au wires, the distances between voltage pads are 203μm and 195μm for samples $b2$ and $b3$ respectively.

Choosing the marker for the position of each contact at the Au wire mid-point, at the edge of the Ag paste or at the intermediate point between the two, leads to a factor of two or three difference in the measured distance between contacts, and therefore in

the absolute value of ρ_b. We believe that the discrepancies between values reported here and those reported previously [12, 14, 15] arise from different conventions adopted to measure the distance between voltage electrodes. In this study, we have used the distance between the mid-point of the Au wires to calculate ρ_b.

References

[1] Kim C, Matsuura A Y, Shen Z-X, Motoyama N, Eisaki H, Uchida S, Tohyama T, and Maekawa S 1996 *Phys. Rev. Lett.* **77** 4054-4057.

[2] Claessen R, Sing M, Schwingenschlögl U, Blaha P, Dressel M and Jacobsen C S 2002 *Phys. Rev. Lett.* **88** 096402.1-4.

[3] Tomonaga S 1950 *Prog. Theor. Phys.* **5** 544-569.

[4] Luttinger J M 1963 *J. Math. Phys.* **4** 1154-1162.

[5] Horii S, Yamada Y, Ikuta H, Yamada N, Kodama Y, Katano S, Funahashi Y Morii S, Matsushita A, Matsumoto T, Hirabayashi I and Mizutani U 1998 *Physica* **302C** 10-22.

[6] Terasaki I, Seiji N, Adachi S, and Yamauchi H 1996 *Phys. Rev. B* **54** 11993-11996.

[7] Horii S, Mizutani U, Ikuta H, Yamada Y, Ye J H, Matsushita A, Hussey N E, Takagi H and Hirabayashi I 2000 *Phys. Rev. B* **61** 6327-6333.

[8] Hussey N E, Kibune M, Nakagawa H, Miura N, Iye Y, Takagi H, Adachi S and Tanabe K 1998 *Phys. Rev. Lett.* **80** 2909-2912.

[9] Moser J, Gabay M, Auban-Senzier P, Jérome D, Bechgaard K, and Fabre J M 1998 *Euro. Phys. J. B* **1** 39-46.

[10] Behnia K, Balicas L, Kang W, Jérome D, Carretta P, Fagot-Revurat Y, Berthier C, Horvatic M, Ségransan P, Hubert L, and Bourbonnais C 1995 *Phys. Rev. Lett.* **74** 5272-5275.

[11] Hussey N E, Mackenzie A P, Cooper J R, Maeno Y, Nishizaki S, and Fujita, T 1998 *Phys. Rev. B* **57** 5505-5511.

[12] Hussey N E, McBrien M N, Balicas L, Brooks J S, Horii S and Ikuta H 2002 *Phys. Rev. Lett.* **89** 086601.1-4.

[13] Vescoli V, Degiorgi L, Henderson W, Grüner G, Starkey K P and Montgomery L K 1998 *Science* **281** 1181-1184.

[14] McBrien M N, Hussey N E, Meeson P J, Horii S and Ikuta H 2002 *J. Phys. Soc. Japan* **71** 701-704.

[15] Nakada K, Ikuta H, Horii S, Nozaki H, Hirabayashi I and Mizutani U 2001 *Physica* **357C-360C** 186-189.

[16] Waku K, Hussey N E, Sakai F, Nohara M, Takagi H, Nakagawa H, Miura N and Adachi S 2000 *J. Phys. Soc. Japan* **69** 21-24.

[17] Gor'kov L P and Lebed A G 1984 *J. Phys. Lett. (France)* **45** L433.

[18] Mackenzie A P, Julian S R, Diver A J, McMullan G J, Ray M P, Lonzarich G G, Maeno Y, Nishizaki S and Fujita T 1996 *Phys. Rev. Lett.* **76** 3786-3789.

[19] Li W-H, Wu S Y, Lin Y-C, Lee K C, Lynn J W, Weng S S, Hong I P, Lin J-Y and Yang H D 2000 *Phys. Rev. B* **60** 4212-4219.

[20] Mott, N F 1990 *Metal-Insulator Transitions* (Taylor & Francis, London).

[21] Kondo J 1964 *Prog. Theor. Phys.* **32** 37-49.

[22] Matsushita Y, Bluhm H, Geballe T H and Fisher I R 2005 *Phys. Rev. Lett.* **94** 157002.1-4.

[23] Ando Y, Boebinger G S, Passner A, Kimura T and Kishio K 1995 *Phys. Rev. Lett.* **75** 4662-4665.

[24] Giamarchi T 2004 *Quantum Physics in One Dimension* (Oxford University Press, New York).

[25] Monod P 1967 *Phys. Rev. Lett.* **19** 1113-1117.

[26] Narduzzo A *et al*, unpublished.

[27] Oshiyama A, Nakao K and Kamimura H 1978 *J. Phys. Soc. Japan* **45** 1136-1146.

[28] Mizokawa T, Kim C, Shen Z-X, Ino A, Yoshida T, Fujimori A, Goto M, Eisaki H, Uchida S, Tagami

M, Yoshida K, Rykov A I, Siohara Y, Tomimoto K, Tajima S, Yamada Y, Horii S, Yamada N, Yamada Y and Hirabayashi I 2000 *Phys. Rev. Lett.* **85** 4779-4782.

[29] Mott N F and Twose, W D 1961 *Adv. Phys.* **10** 107-163.

[30] Ishii, K 1973 *Supp. Prog. Theor. Phys.* **53** 77-138.

[31] Giamarchi T and Schulz H J 1988 *Phys. Rev. B* **37** 325-340.

[32] Kane C L and Fisher, M 1992 *Phys. Rev. Lett.* **68** 1220-1223.

[33] Takenaka K, Nakada K, Osuka A, Horii S, Ikuta H, Hirabayashi I, Sugai S and Mizutani U 2000 *Phys. Rev. Lett.* **85** 5428-5431.

[34] Mizokawa T, Nakada K, Kim C, Shen Z-X, Yoshida T, Fujimori A, Horii S, Yamada Y, Ikuta H and Mizutani U 2002 *Phys. Rev. B* **65** 193101.1-4.

[35] Milliken F P, Umbach C P, and Webb R A 1996 *S. State. Comm* **97** 309-313.

[36] Singleton J, Goddard P A, Ardavan A, Harrison N, Blundell S J, Schlueter J A and Kini A M 2002 *Phys. Rev. Lett.* **88** 037001.1-4.